nature nanotechnology

Article

https://doi.org/10.1038/s41565-024-01685-3

Strong chiroptical nonlinearity in coherently stacked boron nitride nanotubes

Received: 22 August 2023

Accepted: 24 April 2024

Published online: 06 June 2024

Check for updates

Chaojie Ma[1,8], Chenjun Ma[1,8], Chang Liu[2,8], Quanlin Guo[1,8], Chen Huang[1], Guangjie Yao[1], Meiyun Li[3], Jiajie Qi[1], Biao Qin[1], Xin Sui[2], Jiacheng Li[1], Muhong Wu[2], Peng Gao[2], Wenlong Wang[3,4], Xuedong Bai[3,4], Zhipei Sun[5], Enge Wang[2,4,6], Hao Hong[1,7] ✉ & Kaihui Liu[1,2,4] ✉

Nanomaterials with a large chiroptical response and high structural stability are desirable for advanced miniaturized optical and optoelectronic applications. One-dimensional (1D) nanotubes are robust crystals with inherent and continuously tunable chiral geometries. However, their chiroptical response is typically weak and hard to control, due to the diverse structures of the coaxial tubes. Here we demonstrate that as-grown multiwalled boron nitride nanotubes (BNNTs), featuring coherent-stacking structures including near monochirality, homo-handedness and unipolarity among the component tubes, exhibit a scalable nonlinear chiroptical response. This intrinsic architecture produces a strong nonlinear optical response in individual multiwalled BNNTs, enabling second-harmonic generation (SHG) with a conversion efficiency up to 0.01% and output power at the microwatt level—both excellent figures of merit in the 1D nanomaterials family. We further show that the rich chirality of the nanotubes introduces a controllable nonlinear geometric phase, producing a chirality-dependent SHG circular dichroism with values of −0.7 to +0.7. We envision that our 1D chiral platform will enable novel functions in compact nonlinear light sources and modulators.

When intense light interacts with a medium lacking inversion symmetry, the electric dipoles driven by the electromagnetic field in the medium undergo an anharmonic oscillation and produce crucial nonlinear parametric processes such as second-harmonic generation (SHG), spontaneous parametric down-conversion and optical rectification[1,2]. If the medium also breaks mirror symmetry and exhibits chirality, it shows distinct nonlinear responses under different circularly polarized fundamental waves, enabling the control of light polarization in nonlinear processes[3,4]. The manipulation of nonlinear parametric light is highly desirable for various advanced applications in both classical and quantum nonlinear optics, such as optical encryption and security, nonlinear holographic imaging and quantum information process[5–8]. However, there is a trade-off between the high nonlinear susceptibility for efficient SHG output and strong chirality for a large nonlinear chiroptical response (known as SHG circular dichroism (SHG-CD)) in all conventional materials. This trade-off phenomenon primarily arises from the fact that a nonlinear optical crystal usually tends to suppress the chiral effect due to the spatial translational symmetry (except for

[1]State Key Laboratory for Mesoscopic Physics, Frontiers Science Centre for Nano-Optoelectronics, School of Physics, Peking University, Beijing, China. [2]International Centre for Quantum Materials, Collaborative Innovation Centre of Quantum Matter, Peking University, Beijing, China. [3]Institute of Physics, Chinese Academy of Sciences, Beijing, China. [4]Songshan Lake Materials Laboratory, Institute of Physics, Chinese Academy of Sciences, Dongguan, China. [5]QTF Centre of Excellence, Department of Electronics and Nanoengineering, Aalto University, Espoo, Finland. [6]School of Physics, Liaoning University, Shenyang, China. [7]Interdisciplinary Institute of Light-Element Quantum Materials and Research Centre for Light-Element Advanced Materials, Peking University, Beijing, China. [8]These authors contributed equally: Chaojie Ma, Chenjun Ma, Chang Liu, Quanlin Guo. ✉e-mail: haohong@pku.edu.cn; khliu@pku.edu.cn

https://doi.org/10.1038/s41565-024-01685-3

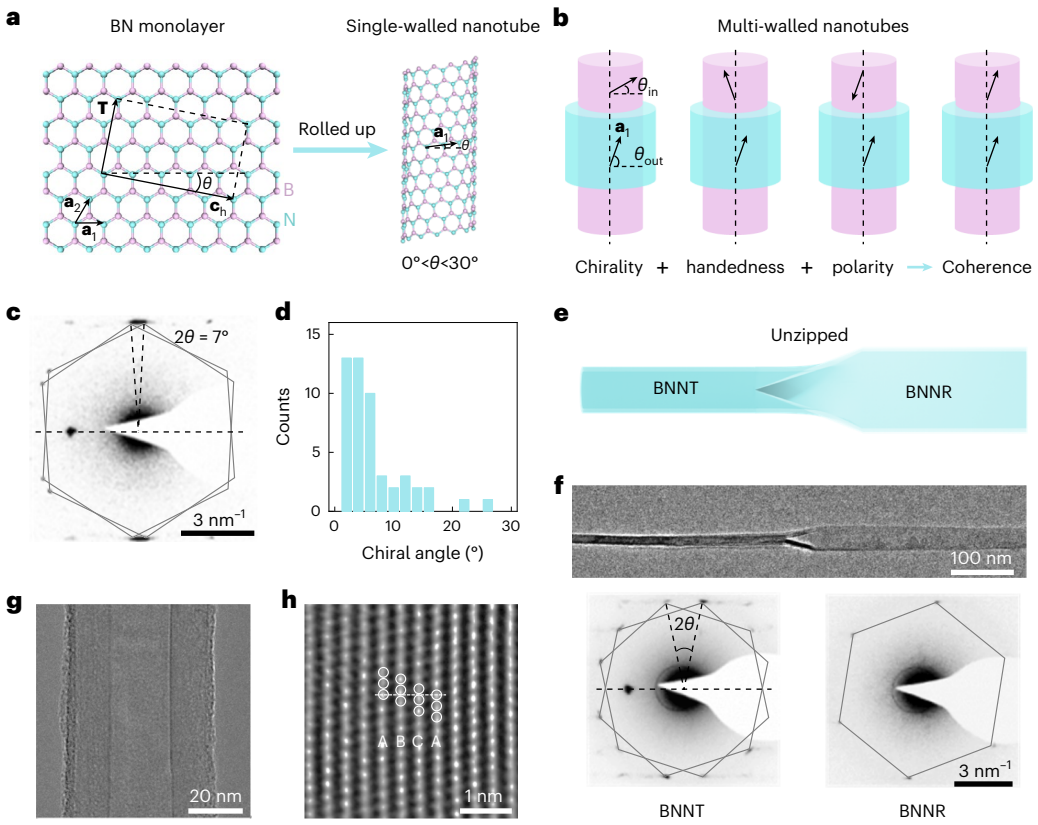

Fig. 1 | Structure of coherently stacked BNNTs. a, Schematic of a BN monolayer rolled up as a single-walled BNNT. θ can be regarded as an angle between vector $\mathbf{a}_1$ and its radial direction. **b**, Intertube stacking configuration in multiwalled BNNTs depending on the chirality, handedness and polarity of each component. Coherence stacking implies uniform chirality, handedness and polarity. **c**, TEM diffraction image of a multiwalled BNNT, indicating the near monochirality with a chiral angle of ~3.5°. **d**, Histogram of the chirality distribution for 50 BNNTs. **e**, Schematic view of a BNNT along a segment unzipped into a BNNR. **f**, TEM image (top) and diffraction images (bottom) of a BNNT after plasma etching to form the multilayer BNNR. Two sets of patterns degenerate to one set after unzipping, indicating the homo-handedness of the BNNT. **g**,**h**, High-resolution TEM image (**g**) and partially enlarged image (**h**) of BNNT. The ABC stacking order indicates the unipolarity between walls in the BNNT.

some special crystals with weak chirality, such as quartz), and an isotropic collection of chiral molecules with high optical activity forbids a strong SHG response[1,2]. Recently, great efforts have been made to overcome this limitation, such as designing artificial chiral nanostructures and incorporating chiral molecules into crystals[9–14]. However, the pursuit of comprehensive SHG performance with both high output and large CD remains an enormous challenge. Thus, exploring intrinsic chiral materials with high stability, strong optical nonlinearity and large chiroptical response is still highly desirable.

Two-dimensional (2D) van der Waals materials with very high nonlinear susceptibilities have attracted intense interest in nonlinear optical regimes[15–17]. When 2D layered materials are rolled up along a defined direction, the formed one-dimensional (1D) nanotubes naturally have intrinsically chiral and highly stable architectures, exhibiting rich physics and enabling novel applications[18–22]. At the same time, the reduced dimensionality further breaks the crystal symmetry and enhances the Coulomb interactions, resulting in spontaneous electric polarization and strong nonlinear optical responses[23–26] (Fig. 1a). However, the chiroptical response is typically quite weak in the whole 1D system. In single-walled nanotubes, the light–matter interaction strength is limited by the atomic-scale thickness[27,28]. In multiwalled nanotubes, the diverse chirality of coaxial tubes (in which the chirality determines crystal symmetry; Supplementary Fig. 1) impedes the scalability of the SHG response with respect to the number of walls[26,29]. Unlike their 2D counterparts, which can be arbitrarily stacked layer by layer to engineer and enhance their nonlinear optical properties[30–35], multiwalled nanotubes entail intertube stacking that is much more complex and simultaneously dependent on the chirality, handedness and polarity of the component tubes (Fig. 1b). The uncontrollable intertube stacking in a multiwalled nanotube consequently diminishes the remarkable physical properties arising from the polar structure of their component nanotubes and thus limits the exploration of their unique chiroptical applications[36,37].

Boron nitride nanotubes (BNNTs) are exemplary and ideal 1D chiral nonlinear optical materials with the merits of wide bandgap, excellent physicochemical stability, large nonlinear susceptibility and high laser damage threshold[38–41]. It has been predicted that a single-walled BNNT can have a large nonlinear susceptibility of the order of 10 pm V^{-1}, and that the chiral structures of the component tubes in multiwalled BNNTs can be correlated[41–44]. Nevertheless, experimental studies on the nonlinear optical responses and structure-dependent chiroptical behaviours of multiwalled BNNTs remain scarce. In this Article, we demonstrate that as-grown multiwalled BNNTs featuring a coherent-stacking configuration with near monochirality, homo-handedness and unipolarity are highly promising materials for constructive enhancement of the nonlinear optical responses of each coaxial tube. This configuration enables strong chiroptical nonlinearity of BNNTs with a giant SHG yield (0.01% conversion efficiency and microwatt output, among the highest reported for 1D materials) as well as an intrinsic and continuously tunable SHG-CD (from −0.7 to +0.7).

Coherently stacked structure in BNNTs

In our experiments, the multiwalled BNNTs were grown via the catalytic chemical vapour deposition method[45,46] (see Methods and

https://doi.org/10.1038/s41565-024-01685-3

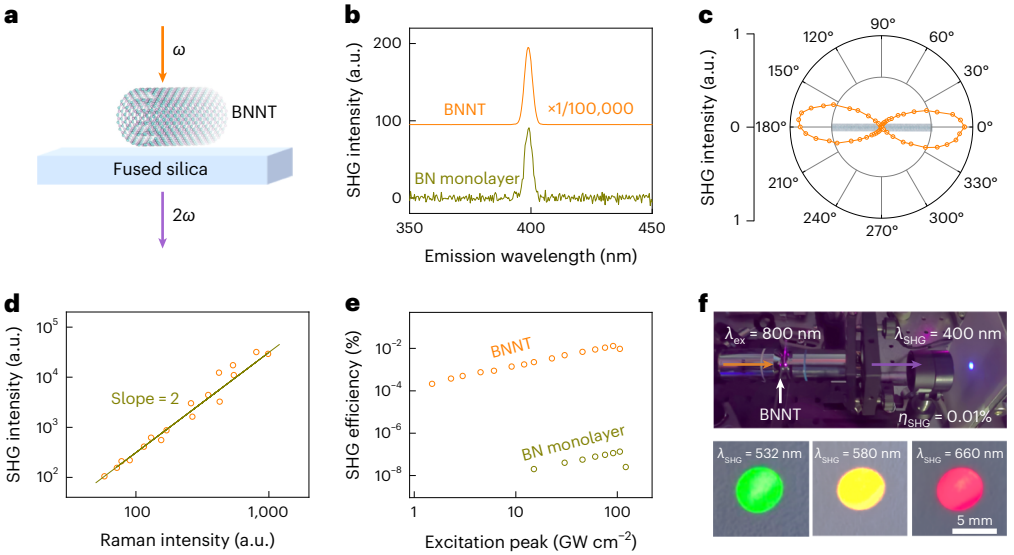

Fig. 2 | Giant SHG response in BNNTs. a, Side-view illustration of a multiwalled BNNT and its SHG response. **b**, SHG spectra of a BNNT and a BN monolayer. Under 800 nm pulsed laser excitation, the SHG signal of the BNNT is five orders of magnitude stronger than that of the BN monolayer. a.u., arbitrary units. **c**, Polarization-dependent SHG patterns of the BNNT as a function of the excitation polarization angle under co-polarized excitation and detection. **d**, SHG intensity versus Raman intensity of multiwalled BNNTs. The SHG intensity is approximately quadratic with the Raman intensity, agreeing with the coherent stacking between coaxial component tubes. **e**, Excitation peak intensity dependence of the SHG conversion efficiency in the BNNT and BN monolayer. The nanotube exhibits an SHG conversion efficiency of up to 0.01% and attains microwatt-level emission power. **f**, Panchromatic SHG response of the BNNT under non-resonant excitation. The generated light at wavelengths of 400 nm, 532 nm, 580 nm and 660 nm is recorded using a camera.

Supplementary Fig. 2 for more details). Transmission electron microscopy (TEM) imaging revealed that the BNNTs were of high purity and almost free from impurities, and their chirality could be characterized by the selected area electron diffraction technique[47] (Supplementary Fig. 3). The diffraction pattern of a multiwalled BNNT showed two sets of hexagonal spots, indicating that all of the walls of this nanotube had a nearly uniform chiral angle of ~3.5° (Fig. 1c). We examined numerous high-quality nanotubes and found that they primarily exhibited single chiral angles. Here, most monochiral BNNTs were axially quasi-zigzag structures (Fig. 1d). To characterize the handedness of each component, we unzipped the multiwalled BNNTs by using a plasma etching method to yield BN nanoribbons (BNNRs; Fig. 1e; see Methods and Supplementary Fig. 4 for more details). After plasma etching, the processed BNNTs were transferred onto TEM grids for characterization; multiwalled BNNT and multilayer BNNR areas were found to coexist (Fig. 1f). The two sets of patterns in BNNT degenerate to one set in the unzipping BNNR area (Fig. 1f), directly validating the homo-handedness of each component for the multiwalled nanotube. Furthermore, we performed high-resolution TEM imaging to characterize the stacking structure of a BNNT (Fig. 1g). The magnified high-resolution TEM image indicated that the walls of the BNNT had the ABC stacking order (Fig. 1h and Supplementary Fig. 3), which resembles the rhombohedral BN (rBN) crystal (Supplementary Fig. 5). Thus, different coaxial walls in the BNNT are expected to have a parallel interlayer stacking order with unipolarity (the B–N bond in each layer is in the same direction, as shown in Supplementary Fig. 1).

Strong optical nonlinearity in BNNTs

The polar structures of the quasi-zigzag BNNTs imply the absence of inversion symmetry and the presence of SHG responses. In the following experiments, we performed SHG measurements in the transmission geometry with BNNTs monodispersed on a fused silica substrate (Fig. 2a). Under 800 nm femtosecond pulse excitation, an individual BNNT exhibited a strong SHG response with a spectral peak at 400 nm (Fig. 2b). The nanotube showed an obvious nonlinear optical anisotropic response due to its reduced dimensionality. Under co-polarized excitation and detection, the polarization-dependent SHG measurement showed a two-petal pattern (Fig. 2c), where the direction of the maximum SHG intensity was nearly parallel to the nanotube axis.

The coherent-stacking configuration will bring a giant SHG enhancement with increasing number of coaxial walls of the BNNTs, because of the constructive interference between walls. Experimentally, we measured the SHG intensity versus the intensity of the Raman G mode at 1,370 cm^{-1} (Supplementary Fig. 6). As the Raman (SHG) intensity corresponds approximately linearly (quadratically) to the number of walls in coherent BNNTs, a quadratic law between the SHG and Raman intensities is expected for the quasi-zigzag nanotubes (Fig. 2d). Additionally, the nonlinear dependence of SHG responses on nanotube diameters (Supplementary Fig. 7) and the constant nonlinear susceptibility across BNNTs (~47 pm V^{-1}; see more details in Supplementary Fig. 8 and Supplementary Note 1) all support the coherent-stacking configuration within BNNTs (Fig. 1b). For a BNNT with a strong Raman signal and an outer diameter of ~350 nm (characterized by atomic force microscopy; Supplementary Fig. 9), the SHG intensity was ~100,000 times stronger than that of the BN monolayer (Fig. 2b). Benefiting from the wide bandgap with a value of ~5.5 eV (refs. 38,39), BNNTs also avoided the resonant excitation of states at the band edge and shallow defects, resulting in a high laser-induced damage threshold of ~90 GW cm^{-2} (~15 mW, comparable to that of the BN monolayer) and a high SHG conversion efficiency ($\eta = P^{2\omega}/P^{\omega}$, where P^{ω} and $P^{2\omega}$ are the powers of the excitation light and SHG light, respectively) of up to 0.01% (Fig. 2e). As a result, an individual BNNT produced a panchromatic SHG output at microwatt power, which could be observed even with the naked eye (Fig. 2f and Supplementary Fig. 9).

The unique structure of the BNNTs also enables strong high-order nonlinear optical responses beyond SHG. Under near-infrared pulsed laser excitation (~0.9 eV), we characterized the high-harmonic-generation (HHG) response in an individual BNNT (Fig. 3a). When compared with a hexagonal BN flake (~60 nm thickness; Supplementary Fig. 10), the HHG processes are much more efficient in the BNNT (Fig. 3b), with up to the sixth order (~5.4 eV) detected. Furthermore, we measured the fourth to sixth HHG intensities as a function of pump intensity I. The nth harmonic

https://doi.org/10.1038/s41565-024-01685-3

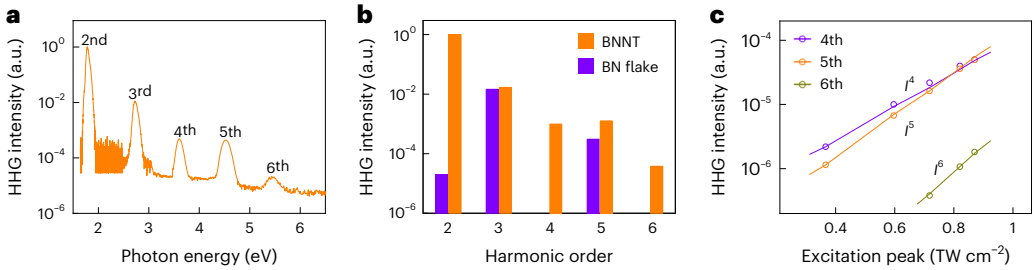

Fig. 3 | HHG response in BNNT. a, HHG spectrum of an individual BNNT. Under excitation light with a photon energy of ~0.9 eV and a peak intensity of ~0.8 TW cm^{-2}, an individual BNNT exhibits the second to sixth harmonic responses, and the highest harmonic is detected with an energy of ~5.4 eV. **b**, Histogram of the HHG intensity of an individual BNNT (~350 nm outer diameter) and a hexagonal BN flake (~60 nm thickness). The BNNT possesses a much more efficient harmonic response. **c**, Pump peak intensity dependence of the fourth to sixth harmonics of the BNNT. The measured *n*th harmonics yield a function of *I* with a power law of I^n, indicating that the HHG response is still in the perturbative regime under our experimental conditions.

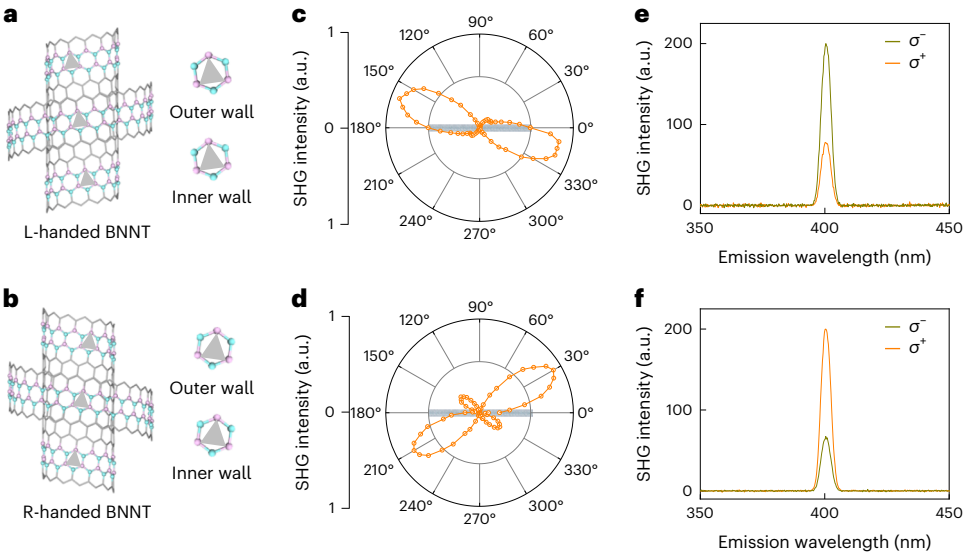

Fig. 4 | Handedness-dependent chiroptical SHG response in BNNTs. **a**,**b**, Schematic geometric structures of L-handed (**a**) and R-handed (**b**) double-walled BNNTs. The two nanotube enantiomers have mirror-symmetric polarity with respect to each other, marked with grey triangles. **c**,**d**, Polarization-dependent SHG patterns of two chiral BNNTs with a clockwise rotation (**c**) and an anti-clockwise rotation (**d**) about the nanotube axis. The patterns are given as a function of the excitation polarization angle under co-polarized excitation and detection and show the deviation between the orientation of maximum response for the parallel SHG component and the nanotube axis. Different rotation orientations of the patterns indicate opposite handedness. **e**,**f**, Chiroptical SHG response of the BNNTs in **c** and **d** under σ^- and σ^+ light excitation. Under 800 nm pulsed laser excitation, the BNNT in **c** exhibits a stronger SHG response with σ^- light excitation, corresponding to the defined L-handed tube, and the BNNT in **d** exhibits a stronger SHG response with σ^+ light excitation, corresponding to the defined R-handed tube.

response yielded an intensity dependence of I^n, indicating that the HHG process was still in the perturbative regime under a pump peak intensity of ~0.8 TW cm^{-2} (Fig. 3c). Given their high cut-off energy, BNNTs could be a promising material for HHG sources for deep-ultraviolet emission[48].

Tunable chiroptical SHG in BNNTs

BNNTs with a relatively large chiral angle are expected to exhibit handedness-dependent optical responses. The two enantiomers (see Supplementary Fig. 1 for the handedness definition), that is, the left-handed (L-handed, Fig. 4a) and right-handed (R-handed, Fig. 4b) ones, have mirror-symmetric polarity orientations with respect to each other. Thus, the polarization-dependent SHG pattern of a chiral BNNT features a twist azimuth angle, in contrast to that of a zigzag BNNT, in which the orientation of the maximum parallel component for the SHG response deviates from the nanotube axis (Supplementary Fig. 11). Notably, the twist SHG pattern has an orientation angle that is related to the chiral angle, but the relationship between them is complex and multifaceted[26]. Two typical SHG patterns with opposite rotation about the tube axis were observed in our experiment, with either clockwise rotation (Fig. 4c) or anti-clockwise rotation (Fig. 4d), indicating the opposite handedness of the BNNTs (Supplementary Fig. 11). Under left circularly polarized (σ^-) and right circularly polarized (σ^+) light excitation, the two nanotube enantiomers exhibited different SHG responses, known as the SHG-CD effect (Fig. 4e,f). The SHG-CD is defined as $[I(\sigma^-) - I(\sigma^+)]/[I(\sigma^-) + I(\sigma^+)]$, where $I(\sigma^-)$ and $I(\sigma^+)$ represent the SHG intensities under excitation with σ^- and σ^+ light, respectively. The SHG-CD values of two representative chiral BNNTs shown in Fig. 4c,d were +0.44 and −0.50, which corresponded to the defined L-handed and R-handed BNNTs, respectively. This nonlinear chiroptical response is comparable to that of most advanced artificial chiral nanostructures[9,12]. Furthermore, BNNTs can simultaneously have the outstanding advantages of a large SHG conversion efficiency of 0.01% and a high nonlinear output power at the microwatt level.

The chiroptical SHG response in BNNTs can be qualitatively described by a simplified physical model. As the sidewalls of the nanotubes contribute weak harmonic responses, we simplify multiwalled BNNTs as two pieces of rBN flakes with a twist angle of 2θ (θ is the chiral angle; Fig. 5a). Under σ^-/σ^+ light excitation, the second-harmonic (SH)

https://doi.org/10.1038/s41565-024-01685-3

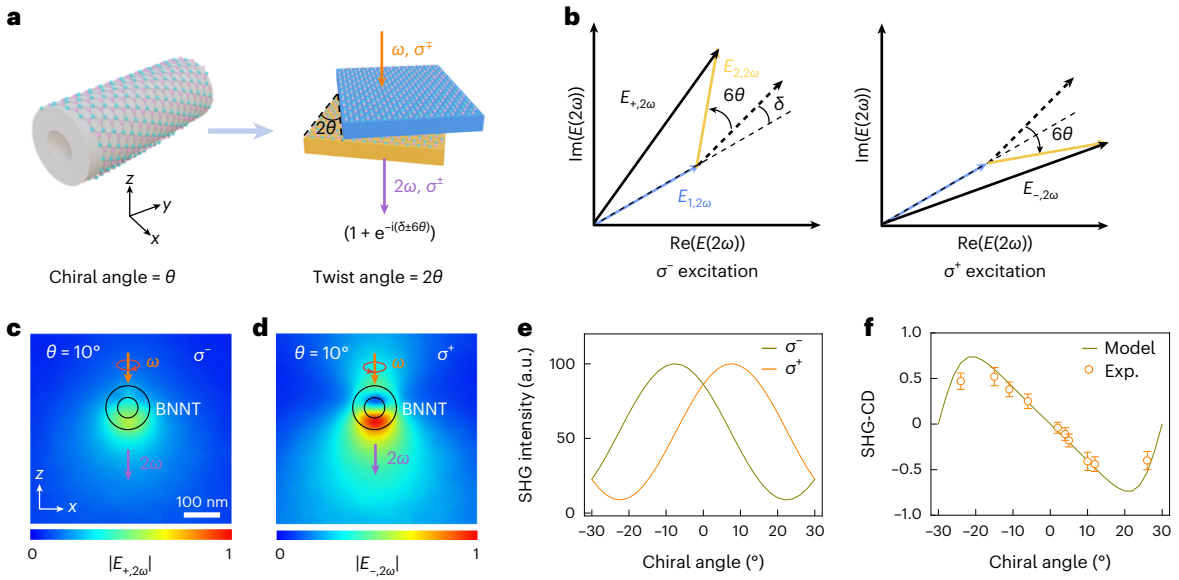

Fig. 5 | Theoretical understanding of the chirality-dependent SHG-CD in BNNTs. a, Schematic of a BNNT with a chiral angle θ (left panel) regarded as twisted rBN flakes with twist angle 2θ (right panel). The blue and yellow flakes correspond to the upper and lower walls of the BNNT. **b**, Complex amplitude diagram illustrating the superposition of the SH electric fields for R-handed twisted rBN ($\theta > 0°$). **c**,**d**, Simulated SH electric field strengths of a BNNT with a chiral angle of 10° under σ^- (**c**) and σ^+ (**d**) light excitation. The SH electric field strength under σ^+ light excitation is stronger. **e**, Simulated chiral SHG intensity of BNNTs with different chiral angles. The chiral structures show an obvious difference in the SHG response under the two circularly polarized light excitations. **f**, Calculated and experimental SHG-CD of BNNTs with different chiral angles. The SHG-CD values are highly correlated with the chiral angles. Experimental data are presented as mean ± s.d. of SHG-CD for each sample from five measurements, where open circles are the mean values and error bars indicate ±s.d.

electric field $E_{\pm,2\omega}$ of the twisted rBN flakes can be written as (see more details in Supplementary Note 2)

$$E_{\pm,2\omega} = \frac{i\sqrt{2}\omega}{cn(2\omega)}\chi E_{\mp,\omega}{}^2\left(e^{-i\Delta k t}-1\right)\left[1+e^{-i(\Delta k t\pm 6\theta)}\right], \quad (1)$$

where ω is the frequency of the fundamental light, c is the velocity of light in vacuum, $n(2\omega)$ is the refractive index of the SH light, χ is the second-order susceptibility of rBN, $E_{\mp,\omega}$ is the electric field of the σ^-/σ^+ fundamental light, $\Delta k = k_{2\omega} - 2k_{\omega}$ is the wavevector mismatch between the fundamental light and SH light, t is the wall thickness, $\delta = \Delta k\, t$ corresponds to a phase mismatch factor and 6θ is the nonlinear geometric phase arising from interlayer twist. According to this model, $E_{\pm,2\omega}$ for a R-handed BNNT can be directly analysed from the complex amplitude diagram (Fig. 5b). In the diagram, the intersection angle between $E_{1,2\omega}$ (SH electric field contributed by the top flake) and $E_{2,2\omega}$ (SH electric field contributed by the bottom flake) is $\delta + 6\theta$ or $\delta - 6\theta$, under σ^- or σ^+ light excitation. The completely opposite nonlinear geometric phase caused by σ^-/σ^+ light excitation and the inherent phase mismatch factor co-determine the nonlinear chiroptical response. Thus, the SHG-CD can be simplified as a function of 2θ and t (Supplementary Fig. 12).

To quantitatively describe the chiroptical SHG response in BNNTs, the effects of intrinsic curvature and nanocavities formed by the nanotubes should be carefully considered. First, we calculated the nonlinear susceptibility tensor of the BNNT by establishing a rolled-up BN model (see more details in Supplementary Note 3). The inhomogeneous nonlinear polarizations P_x and P_y, depending on θ and the azimuth angle α of the nanotube, can be expressed as

$$\begin{cases} P_{x,2\omega}(\theta,\alpha) \\ = \chi\left[-\sin 3\theta\cos^3\alpha\, E_x{}^2 + \sin 3\theta\cos\alpha\, E_y{}^2 - 2\cos 3\theta\cos^2\alpha\, E_x E_y\right] \\ P_{y,2\omega}(\theta,\alpha) \\ = \chi\left[-\cos 3\theta\cos^2\alpha\, E_x{}^2 + \cos 3\theta\, E_y{}^2 + 2\sin 3\theta\cos\alpha\, E_x E_y\right] \end{cases}, \quad (2)$$

where E_x and E_y are the electric fields of the fundamental light perpendicular and parallel to the nanotube axis, respectively. Then, we performed the three-dimensional finite-element simulations using COMSOL Multiphysics to obtain the corresponding SH electric field. From the simulation, we found that the multireflection effect in the nanotube was quite pronounced, leading to a non-uniform distribution of the fundamental light electric field within the tube (Supplementary Fig. 13). Taking all the factors into consideration, we simulated the SH electric fields $E_{+,2\omega}$ (Fig. 5c) and $E_{-,2\omega}$ (Fig. 5d) under σ^- and σ^+ light excitation for a 10° chiral BNNT (with an outer tube diameter of 120 nm and an inner tube diameter of 50 nm). A notably higher SHG output can be observed for the σ^+ excitation, with an SHG-CD of −0.40. Moreover, we conducted simulations to explore the SHG responses of BNNTs with continuously varying chiral geometries, where the SHG intensities and corresponding SHG-CD values evolved with the chiral angles (Fig. 5e,f). The absolute value of the maximum SHG-CD reached 0.73. Experimentally, we measured the SHG-CD values for several BNNT samples on TEM grids (chiral angles determined by TEM) and found good agreement with the simulation (Fig. 5f).

Conclusions

In summary, our results reveal the unique feature of coherently stacked BNNTs, which preserve both the inversion and mirror asymmetries of the component nanotubes and enable scalable optical nonlinearity. A comprehensive performance of a giant SHG yield (0.01% conversion efficiency, microwatt output) and a simultaneous large SHG-CD (continuously tunable from −0.7 to +0.7) can be achieved (see Supplementary Tables 1 and 2 for comparison with different materials). This capability can be expanded to other second-order nonlinear optical process, such as spontaneous parametric down-conversion, to generate entangled photon pairs with tunable entanglement characteristics[49]. Furthermore, the intrinsic chirality and strong nonlinearity together with the spontaneous electric polarization and abundant stacking configurations in 1D nanotubes are expected to bring much richer physics beyond 2D systems, such as chiral shift current[23], non-reciprocal superconductivity[36] and bulk photovoltaic effect[37]. Our study of the

coherent assembly of chiral nanotubes should motivate further efforts in exploring stacking-engineered physics and applications in 1D nanotube systems.

Online content

Any methods, additional references, Nature Portfolio reporting summaries, source data, extended data, supplementary information, acknowledgements, peer review information; details of author contributions and competing interests; and statements of data and code availability are available at https://doi.org/10.1038/s41565-024-01685-3.

References

1. Shen, Y. R. *The Principles of Nonlinear Optics* (Wiley, 1984).
2. Boyd, R. W. *Nonlinear Optics* (Academic, 2008).
3. Haupert, L. M. & Simpson, G. J. Chirality in nonlinear optics. *Annu. Rev. Phys. Chem.* **60**, 345–365 (2009).
4. Lapine, M., Shadrivov, I. V. & Kivshar, Y. S. Colloquium: nonlinear metamaterials. *Rev. Mod. Phys.* **86**, 1093–1123 (2014).
5. Keren-Zur, S., Michaeli, L., Suchowski, H. & Ellenbogen, T. Shaping light with nonlinear metasurfaces. *Adv. Opt. Photon.* **10**, 309–353 (2018).
6. Wang, M. J. et al. Nonlinear chiroptical holography with Pancharatnam–Berry phase controlled plasmonic metasurface. *Laser Photon. Rev.* **16**, 2200350 (2022).
7. Lodahl, P. et al. Chiral quantum optics. *Nature* **541**, 473–480 (2017).
8. Koshelev, K., Tonkaev, P. & Kivshar, Y. Nonlinear chiral metaphotonics: a perspective. *Adv. Photon.* **5**, 064001 (2023).
9. Li, G., Zhang, S. & Zentgraf, T. Nonlinear photonic metasurfaces. *Nat. Rev. Mater.* **2**, 17010 (2017).
10. Yuan, C. Q. et al. Chiral lead halide perovskite nanowires for second-order nonlinear optics. *Nano Lett.* **18**, 5411–5417 (2018).
11. Long, G. K. et al. Chiral-perovskite optoelectronics. *Nat. Rev. Mater.* **5**, 423–439 (2020).
12. Chen, Y. et al. Multidimensional nanoscopic chiroptics. *Nat. Rev. Phys.* **4**, 113–124 (2021).
13. Han, Z., Wang, F., Sun, J., Wang, X. & Tang, Z. Recent advances in ultrathin chiral metasurfaces by twisted stacking. *Adv. Mater.* **35**, e2206141 (2022).
14. Fu, X. W. et al. Highly anisotropic second-order nonlinear optical effects in the chiral lead-free perovskite spiral microplates. *Nano Lett.* **23**, 606–613 (2023).
15. Li, Y. L. et al. Probing symmetry properties of few-layer MoS_2 and h-BN by optical second-harmonic generation. *Nano Lett.* **13**, 3329–3333 (2013).
16. Autere, A. et al. Nonlinear optics with 2D layered materials. *Adv. Mater.* **30**, e1705963 (2018).
17. Hong, H. et al. Giant enhancement of optical nonlinearity in two-dimensional materials by multiphoton-excitation resonance energy transfer from quantum dots. *Nat. Photon.* **15**, 510–515 (2021).
18. Tenne, R., Margulis, L., Genut, M. & Hodes, G. Polyhedral and cylindrical structures of tungsten disulfide. *Nature* **360**, 444–446 (1992).
19. Chopra, N. G. et al. Boron nitride nanotubes. *Science* **269**, 966–967 (1995).
20. Saitoo, R., Dresselhaus, G. & Dresselhaus, M. S. *Physical Properties of Carbon Nanotubes* (Imperial College Press, 1998).
21. Xiang, R. et al. One-dimensional van der Waals heterostructures. *Science* **367**, 537–542 (2020).
22. Zhao, B. et al. High-order superlattices by rolling up van der Waals heterostructures. *Nature* **591**, 385–390 (2021).
23. Kral, P., Mele, E. J. & Tomanek, D. Photogalvanic effects in heteropolar nanotubes. *Phys. Rev. Lett.* **85**, 1512–1515 (2000).
24. Lucking, M. C., Beach, K. & Terrones, H. Large second harmonic generation in alloyed TMDs and boron nitride nanostructures. *Sci. Rep.* **8**, 10118 (2018).
25. Qian, Q. et al. Chirality-dependent second harmonic generation of MoS_2 nanoscroll with enhanced efficiency. *ACS Nano* **14**, 13333–13342 (2020).
26. Xia, H. M. et al. Probing the chiral domains and excitonic states in individual WS_2 tubes by second-harmonic generation. *Nano Lett.* **21**, 4937–4943 (2021).
27. Sato, N., Tatsumi, Y. & Saito, R. Circular dichroism of single-wall carbon nanotubes. *Phys. Rev. B* **95**, 155436 (2017).
28. Yao, F. R. et al. Complete structural characterization of single carbon nanotubes by Rayleigh scattering circular dichroism. *Nat. Nanotechnol.* **16**, 1073–1078 (2021).
29. Leven, I., Guerra, R., Vanossi, A., Tosatti, E. & Hod, O. Multiwalled nanotube faceting unravelled. *Nat. Nanotechnol.* **11**, 1082–1086 (2016).
30. Yao, K. et al. Enhanced tunable second harmonic generation from twistable interfaces and vertical superlattices in boron nitride homostructures. *Sci. Adv.* **7**, eabe8691 (2021).
31. Zhao, M. et al. Atomically phase-matched second-harmonic generation in a 2D crystal. *Light Sci. Appl.* **5**, e16131 (2016).
32. Du, L. et al. Engineering symmetry breaking in 2D layered materials. *Nat. Rev. Phys.* **3**, 193–206 (2021).
33. Abdelwahab, I. et al. Giant second-harmonic generation in ferroelectric $NbOI_2$. *Nat. Photon.* **16**, 644–650 (2022).
34. Guo, Q. et al. Ultrathin quantum light source with van der Waals $NbOCl_2$ crystal. *Nature* **613**, 53–59 (2023).
35. Yang, D. et al. Spontaneous-polarization-induced photovoltaic effect in rhombohedrally stacked MoS_2. *Nat. Photon.* **16**, 469–474 (2022).
36. Qin, F. et al. Superconductivity in a chiral nanotube. *Nat. Commun.* **8**, 14465 (2017).
37. Zhang, Y. J. et al. Enhanced intrinsic photovoltaic effect in tungsten disulfide nanotubes. *Nature* **570**, 349–353 (2019).
38. Blase, X., Rubio, A., Louie, S. G. & Cohen, M. L. Stability and band gap constancy of boron nitride nanotubes. *Europhys. Lett.* **28**, 335–340 (1994).
39. Golberg, D., Bando, Y., Tang, C. C. & Zhi, C. Y. Boron nitride nanotubes. *Adv. Mater.* **19**, 2413–2432 (2007).
40. Cohen, M. L. & Zettl, A. The physics of boron nitride nanotubes. *Phys. Today* **63**, 34–38 (2010).
41. Guo, G. Y. & Lin, J. C. Second-harmonic generation and linear electro-optical coefficients of BN nanotubes. *Phys. Rev. B* **72**, 075416 (2005).
42. Margulis, V. A., Muryumin, E. E. & Gaiduk, E. A. Second-order nonlinear optical response of zigzag BN single-walled nanotubes. *Phys. Rev. B* **82**, 235426 (2010).
43. Golberg, D., Bando, Y., Bourgeois, L., Kurashima, K. & Sato, T. Insights into the structure of BN nanotubes. *Appl. Phys. Lett.* **77**, 1979–1981 (2000).
44. Celik-Aktas, A., Zuo, J. M., Stubbins, J. F., Tang, C. & Bando, Y. Structure and chirality distribution of multiwalled boron nitride nanotubes. *Appl. Phys. Lett.* **86**, 133110 (2005).
45. Tang, C., Bando, Y., Sato, T. & Kurashima, K. A novel precursor for synthesis of pure boron nitride nanotubes. *Chem. Commun.* **12**, 1290–1291 (2002).
46. Bai, X. D. et al. Deformation-driven electrical transport of individual boron nitride nanotubes. *Nano Lett.* **7**, 632–637 (2007).
47. Liu, K. et al. Direct determination of atomic structure of large-indexed carbon nanotubes by electron diffraction: application to double-walled nanotubes. *J. Phys. D* **42**, 125412 (2009).

48. Tancogne-Dejean, N. & Rubio, A. Atomic-like high-harmonic generation from two-dimensional materials. *Sci. Adv.* **4**, eaao5207 (2018).
49. Tang, H. et al. An on-chip platform for multi-degree-of-freedom control of two-dimensional quantum. Preprint at https://doi.org/10.48550/arXiv.2311.12030 (2023).

Methods

Sample preparation

BNNTs were synthesized in a vertical induction furnace using the previously reported catalytic chemical vapour deposition method[45,46] (see Supplementary Fig. 2 for more details). After growth, the high-purity BNNTs were dissolved in ethyl alcohol by ultrasonication for 30 min, a process that enabled us to isolate individual BNNTs. We find that these nanotubes show a predominant diameter of 30–60 nm and we also see the occurrence of BNNTs with diameters greater than 100 nm. The resulting BNNT suspension could be applied to substrates such as fused silica for optical measurement or a grid for TEM characterization. Here, the straight and high-quality ones are meticulously selected for further characterization from optical images. It should be mentioned that not all samples are perfect with coherently stacking walls (~20% are not good). The outer diameter, wall thickness and chirality of the BNNTs might be controlled by the growth conditions of temperature, catalyst concentration and so on[50–52]. In addition, we processed multiwalled BNNTs through the plasma etching method[53] to form BNNRs (Supplementary Fig. 4). During this process, BNNTs were first deposited on a substrate and then coated with a polymethylmethacrylate film. Subsequently, the polymethylmethacrylate–BNNT composite was picked up and flipped over, and subjected to Ar plasma etching to create nanoribbons. After etching, the composite film was transferred onto TEM grids through the dry-transfer technique. Finally, polymethylmethacrylate was removed by high-temperature annealing to release BNNRs onto grids for TEM characterization.

Sample characterization

Optical images were taken with an Olympus BX51M microscope. Raman spectra were measured using a custom-designed confocal microscope optical system with an excitation wavelength of 514 nm. TEM (FEI Titan Themis G2 300) was conducted to characterize the structure and chiral angle. Atomic force microscopy measurements were performed using an Asylum Research Cypher in an ambient atmosphere. Scanning electron microscopy images were obtained using a Thermo Fisher Helios G4 UX.

Harmonic-generation measurements

A mode-locked Ti:sapphire oscillator (Coherent Mira-HP, ~130 fs, 76 MHz) equipped with an optical parametric oscillator (Coherent Mira-OPO-X) was used as the laser system for SHG measurement. The excitation laser beam was focused using an Olympus objective (100×; numerical aperture (NA) = 0.90), and its polarization was controlled by a half-wave plate. The spot diameter of the excited light with a wavelength of 800 nm on the sample is ~1 μm. The SHG signals were collected in the transmission mode by the Olympus objective (40×, NA = 0.65). After filtering out the excitation laser, the SHG signal was recorded using a spectrometer equipped with a nitrogen-cooled silicon CCD (charge-coupled device) camera (Princeton SP2500). In the chiral SHG measurement, the half-wave plate was replaced by a quarter-wave plate. The generated circularly polarized light (800 nm) was calibrated using a Thorlabs polarimeter (PAX1000IR1). The definition of a left-handed (right-handed) nanotube corresponds to a stronger SHG response under left (right) circularly polarized light excitation. In the HHG measurement system, femtosecond pulses (~70 fs, 250 kHz) with an energy of ~0.90 eV were generated by a Ti:sapphire oscillator (Coherent, Vitara-T) equipped with an optical parametric amplifier (Coherent, 9850). The excitation laser was focused using a reflective objective (40×, NA = 0.50) and the HHG signal was collected in the transmission mode by the second reflective objective (40×, NA = 0.50). The signal was recorded using a spectrometer equipped with a thermoelectric cooling CCD camera (Andor DU420A-BU2).

Numerical simulation

The SHG emission for an individual BNNT is numerically simulated using a frequency-domain finite-element solver in COMSOL Multiphysics based on a wave optics module. To match experimental conditions, the excitation light is modelled using a Gaussian beam with a wavelength of 800 nm and a spot diameter of 1 μm on the tube plane. The linearly or circularly polarized excitation light propagates along the negative direction of the *z* axis. The nanotube is modelled using a hollow cylinder. The nonlinear susceptibility tensors at different azimuth angles of the nanotube are calculated through tensor transformation, which is used as input into the model to generate second-order polarization. Simulations are performed with the scattering boundary and impedance boundary conditions. Two steps are conducted to obtain the ultimate SH electric field distribution. First, the electric field distribution of fundamental light after illuminating the nanotube is obtained. Second, the SH electric field distribution is calculated from the obtained electric field distribution of fundamental light. The SHG intensity is obtained by integrating the signal in the SHG emission core.

Data availability

The data supporting the findings of this study are presented within the paper and Supplementary Information. Additional data are available from the corresponding authors upon reasonable request. Source data are provided with this paper.

References

50. Pakdel, A., Zhi, C. Y., Bando, Y., Nakayama, T. & Golberg, D. A comprehensive analysis of the CVD growth of boron nitride nanotubes. *Nanotechnology* **23**, 215601 (2012).
51. Yang, F. et al. Chirality-specific growth of single-walled carbon nanotubes on solid alloy catalysts. *Nature* **510**, 522–524 (2014).
52. An, Q. et al. Direct growth of single-chiral-angle tungsten disulfide nanotubes using gold nanoparticle catalysts. *Nat. Mater.* **23**, 347–355 (2024).
53. Jiao, L., Zhang, L., Wang, X., Diankov, G. & Dai, H. Narrow graphene nanoribbons from carbon nanotubes. *Nature* **458**, 877–880 (2009).

Acknowledgements

This work was supported by the National Key R&D Program of China (2022YFA1403504 (K.L.)), National Natural Science Foundation of China (52025023 (K.L.), 12374167 (H.H.), 51991342 (K.L.), 62305003 (Chaojie Ma) and 92163206 (M.W.)), Guangdong Major Project of Basic and Applied Basic Research (2021B0301030002 (E.W. and K.L.)), Strategic Priority Research Program of Chinese Academy of Sciences (XDB33000000 (K.L.)), China Postdoctoral Science Foundation (2022M710232 (C.L.)) and New Cornerstone Science Foundation through the XPLORER PRIZE (K.L.).

Author contributions

K.L. and H.H. supervised and conceived the projects. Chaojie Ma and C.L. performed the SHG and HHG experiments. Chaojie Ma and Chenjun Ma performed the chiroptical measurement. Chenjun Ma, H.H., C.H., J.L. and Z.S. contributed the theoretical calculations. Q.G., M.W., P.G. and X.B. conducted the TEM experiments. M.L., X.S. and W.W. prepared and processed BNNT samples. Q.G., J.Q. and B.Q. conducted the scanning electron microscopy and atomic force microscopy measurements. G.Y., Z.S. and E.W. suggested the optical experiments. All the authors discussed and contributed to writing the paper.

Competing interests

The authors declare no competing interests.

Additional information

Supplementary information The online version contains supplementary material available at https://doi.org/10.1038/s41565-024-01685-3.

Correspondence and requests for materials should be addressed to Hao Hong or Kaihui Liu.

Peer review information *Nature Nanotechnology* thanks Qinwei An, Shengxi Huang and Enrique Diez for their contribution to the peer review of this work.